Measurement of the mass energy-absorption coefficient of air for x-rays in the range from 3 to 60 keV

2012 Phys. Med. Biol. 57 8231

(http://iopscience.iop.org/0031-9155/57/24/8231)

IOP PUBLISHING PHYSICS IN MEDICINE AND BIOLOGY

Phys. Med. Biol. **57** (2012) 8231–8247 doi:10.1088/0031-9155/57/24/8231

Measurement of the mass energy-absorption coefficient of air for x-rays in the range from 3 to 60 keV

H Buhr[1], **L Büermann**[1], **M Gerlach**[2], **M Krumrey**[2] **and H Rabus**[1]

[1] Physikalisch-Technische Bundesanstalt, Bundesallee 100, D-38116 Braunschweig, Germany
[2] Physikalisch-Technische Bundesanstalt, Abbestrasse 2-12, D-10587 Berlin, Germany

E-mail: henrik.buhr@ptb.de and ludwig.bueermann@ptb.de

Received 15 August 2012, in final form 25 October 2012
Published 29 November 2012
Online at stacks.iop.org/PMB/57/8231

Abstract

For the first time the absolute photon mass energy-absorption coefficient of air in the energy range of 10 to 60 keV has been measured with relative standard uncertainties below 1%, considerably smaller than those of up to 2% assumed for calculated data. For monochromatized synchrotron radiation from the electron storage ring BESSY II both the radiant power and the fraction of power deposited in dry air were measured using a cryogenic electrical substitution radiometer and a free air ionization chamber, respectively. The measured absorption coefficients were compared with state-of-the art calculations and showed an average deviation of 2% from calculations by Seltzer. However, they agree within 1% with data calculated earlier by Hubbell. In the course of this work, an improvement of the data analysis of a previous experimental determination of the mass energy-absorption coefficient of air in the range of 3 to 10 keV was found to be possible and corrected values of this preceding study are given.

(Some figures may appear in colour only in the online journal)

1. Introduction

Effects of ionizing radiation on matter are usually quantified in terms of the absorbed dose. For indirectly ionizing radiation like x-rays the absorbed dose D is linked to the kerma K (kinetic energy released per mass). The kerma is the quotient of the mean sum of the initial kinetic energies of all charged particles liberated by incident uncharged particles in a volume of a material and the mass of this material.

Air kerma free-in-air can be measured with low uncertainty with free air ionization chambers which are in use at many national metrology institutes around the world as primary standards (Burns and Büermann 2009). In many practical applications, the absorbed dose to

materials other than air is of interest, e.g. to water or biological tissue, calling for a method to convert measured values of air kerma free-in-air into absorbed dose to other media. If certain conditions are met, the absorbed dose can be well approximated by the kerma, i.e. if the medium consists of low-Z atoms, the energy of the photons is below 300 keV and the *secondary electron equilibrium* prevails. Under these circumstances the *kerma approximation* holds because (i) the fraction g of kinetic energy lost in bremsstrahlung by the secondary electrons that are released by the primary photon interactions is negligible and (ii) the ranges of secondary electrons are much shorter than those of the primary and scattered photons. The total kerma minus the energy lost to bremsstrahlung of secondary electrons is known as collision kerma $K_{C,A}$ (Attix 1979) of medium A, which is given by

$$K_{C,A} = \psi(E)(\mu_{en}(E)/\rho)_A \tag{1}$$

where $\psi(E)$ is the photon energy fluence for photon energy E, $(\mu_{en}/\rho)_A$ is the mass energy-absorption coefficient of material A and ρ is its density (ICRU 2011). Within the limits of the kerma approximation, the collision kerma is equal to the absorbed dose D_A to the medium A. Furthermore, provided that the conditions of the kerma approximation hold for another medium B, the absorbed dose D_B in medium B relates to D_A by

$$D_B = D_A \times \frac{(\mu_{en}(E)/\rho)_B}{(\mu_{en}(E)/\rho)_A} \tag{2}$$

for a given photon energy fluence. Despite the importance of (μ_{en}/ρ) for photon dosimetry, experimental values for this quantity are largely unavailable with only few exceptions (Bradley *et al* 1989, Singh *et al* 1991, Büermann *et al* 2006) whereas calculations are available for almost all elements (e.g. Hubbell 1982, Seltzer 1993, Berger *et al* 2010). A very recent theoretical study by Andreo *et al* (2012) looked into the uncertainty of photon mass energy-absorption coefficients and their ratios in radiation dosimetry and found, similar to what was observed by Büermann *et al* (2006), that the experimental data is better described, if re-normalization factors for photoelectric cross sections that are neglected in the more recent calculations are applied, as had been done by Hubbell (1982).

In this work, the photon–energy dependent function used to convert the measured charges by the free air chamber into the energy deposited in air takes into account the complete correction for the number of electrons liberated in the photon interactions (or the charge of the ions produced thereby) that was pointed out in a recent work of Takata and Begum (2008). In general, this conversion function can also be applied to convert the frequently used quantity exposure into air kerma (ICRU 2011). Furthermore, the improved conversion function was applied to re-evaluate results previously published by Büermann *et al* (2006) and led to relative differences in the mass energy-absorption coefficient of air between 1% at 3 keV and 0.4% at 10 keV. The improved data are provided in the appendix.

2. Method and instrumentation

2.1. Definition of interaction coefficients

The method used to measure mass energy-absorption coefficients of air can be derived from the definitions of interaction coefficients as given by the ICRU (2011). The *mass energy-transfer coefficient*, μ_{tr}/ρ, of a material for uncharged particles of a given type and energy is the quotient of $\mathrm{d}R_{tr}/R$ by $\rho\,\mathrm{d}l$, where $\mathrm{d}R_{tr}$ is the mean energy that is transferred to kinetic energy of charged particles by interactions of the uncharged particles of incident radiant energy R in traversing a distance $\mathrm{d}l$ in the material of density ρ, thus,

$$\frac{\mu_{tr}}{\rho} = \frac{1}{\rho\,\mathrm{d}l}\frac{\mathrm{d}R_{tr}}{R}. \tag{3}$$

The product of μ_{tr}/ρ and $(1 - g)$ where g is the fraction of the energy of the liberated charged particles that is subsequently lost in radiative processes in the material is called the *mass energy-absorption coefficient* μ_{en}/ρ of the material. Similar to equation (3) μ_{en}/ρ can be written as

$$\frac{\mu_{en}}{\rho} = \frac{1}{\rho\,\mathrm{d}l}\frac{\mathrm{d}R_{en}}{R} \tag{4}$$

where $\mathrm{d}R_{en} = \mathrm{d}R_{tr}(1 - g)$. For photons with energies below 60 keV, g in air is less than 0.01%. Therefore, for the photon energies investigated in the present work μ_{tr}/ρ and μ_{en}/ρ can be regarded as being virtually equal. From equation (4) it is obvious that the following components are needed for the measurement of the mass energy-absorption coefficient of air for photons: (i) a monoenergetic photon beam, (ii) a device to measure the radiant energy R and (iii) a device to measure $\mathrm{d}R_{en}/(\rho\,\mathrm{d}l)$. In the present work we make use of monochromatized synchrotron radiation in the range from 8 to 60 keV available at the BAMline at the electron storage ring BESSY II (section 2.2), the cryogenic radiometer SYRES I or silicon photodiodes calibrated against the cryogenic radiometer to measure R (sections 2.3 and 2.4) and the free air ionization chamber PK100 to measure $\mathrm{d}R_{en}/(\rho\,\mathrm{d}l)$ (section 2.5).

2.2. 7 T-wavelength-shifter beamline at BESSY II

To determine the energy dependence of the x-ray mass energy-absorption coefficient, monochromatic x-rays are required. Synchrotron radiation beamlines provide tuneable monochromatic radiation with small energy band width and a high photon flux. PTB operates several beamlines for metrological applications of synchrotron radiation in its own laboratory at the electron storage ring BESSY II in Berlin, Germany (Beckhoff *et al* 2009). At the BAMline, a 7 T-wavelength-shifter beamline jointly operated by the Federal Institute for Materials Research and Testing (BAM) and PTB, photon energies between 8 and 60 keV can be selected (Görner *et al* 2001). A double multilayer monochromator (DMM) and a double crystal monochromator (DCM) were used in series for photon energies from 8 to 30 keV to combine a high spectral resolution and higher order contributions of below 10^{-3} even in terms of power. Above 30 keV, the high spectral purity is already achieved by the DCM. The relative spectral bandwidth is about 10^{-3}. The photon energy scale was calibrated to better than 15 eV over the entire range from 8 to 60 keV by using the well-known energies of the K absorption edges of appropriate elements (e.g. Mo, In, Gd, or Ta). At the BAMline the experimental setup is not attached to the vacuum system of the beamline but is under atmospheric air conditions. The beam size was about 1 mm × 1 mm, thus, much smaller than the aperture of all detectors used for the measurements described here. An additional ion chamber or a photodiode, respectively, were operated in transmission mode to monitor the radiant power decrease due to the decreasing current in the storage ring or possible variations caused by the monochromators.

2.3. Cryogenic electrical substitution radiometer SYRES I

Cryogenic electrical substitution radiometers are well established as high accuracy primary detector standards in radiometry. Their working principle is based on the equivalence of radiant power and electrical power required to keep a radiation absorber, typically a cavity, at a fixed temperature slightly above liquid-He temperature. Their range of operation reaches from the infrared and visible to the UV and soft x-ray region. At PTB the usable spectral range was successfully extended to cover hard x-rays with photon energies up to 60 keV (Gerlach *et al* 2008).

2.3.1. The cryogenic electrical substitution radiometer SYRES I as the primary standard in radiometry. The cryogenic electrical substitution radiometer SYRES I with its former copper absorber had been the primary detector standard of PTB to determine the radiant power of monochromatized synchrotron radiation in the photon energy range from 50 eV to 20 keV. Its main field of application is the calibration of semiconductor photodiodes with low uncertainties of typically less than 0.5%. In earlier measurements it was already used together with the free air ionization chamber PK100 to determine the mass energy-absorption coefficient of air up to 10 keV (Büermann *et al* 2006).

During the last decade it underwent a comprehensive modification that resulted in a novel cavity absorber with a 730 μm gold base instead of 100 μm copper, combined with a gold plated copper shell to optimize the thermal properties. This allowed the extension of the useable spectral range up to hard x-ray radiation of 60 keV with an absorptance α_{Cav} between 99.99(1)% below 10 keV and 99.5(1)% at 60 keV (Gerlach *et al* 2008). Extensive Monte Carlo simulations using the Geant4 toolkit (Agostinelli *et al* 2003) especially for scattering and fluorescence effects were performed for the optimization. Experiments for different test geometries were used to validate the simulation code for this application (Gerlach *et al* 2009).

2.3.2. Application of SYRES I in the experiment. The radiant power P of the photon beam is given as

$$P(E) = \int \dot{\psi}(E, A)\, \mathrm{d}A \tag{5}$$

where A is the absorber cross section of the cryogenic radiometer which is large enough to cover the beam and $\dot{\psi}(E, A)$ the position dependent photon energy fluence rate at energy E. Alternatively, it can be written as

$$P = P_{\mathrm{el}}/\alpha_{Cav} \tag{6}$$

where P_{el} is the reduction in electrical power needed for keeping the absorber temperature constant during irradiation with radiant power P and α_{Cav} the absorption coefficient of the cavity absorber. For the measurement at the BAMline the vacuum vessel housing SYRES I had to be sealed off from the ambient air at which the free air ionization chamber was operated by a PF60 beryllium entrance window with a thickness of 0.400(25) mm.

2.4. Silicon photodiodes

Silicon photodiodes can be used as transfer detector standards in the entire x-ray range even without bias voltage. Photodiodes were used in some measurements presented in this work (section 4.3) and their energy-dependent responsivity, defined as the ratio of the induced photocurrent to the incident radiant power, was determined by comparison to the cryogenic radiometer. The use of transfer standards at lower photon energies was necessary because of technical reasons which are discussed in section 4.3.

The photocurrents of the diodes were measured with calibrated picoamperemeters (Keithley 617). The advantages of the photodiodes are their small size (typically 15 mm × 15 mm × 3 mm including packaging), their easy operation in air and in vacuum and the resulting simple positioning in the beam. Different types of silicon photodiodes have been investigated with respect to responsivity, linearity and homogeneity (Krumrey *et al* 2006). The photodiodes used for the measurements and their properties are presented in table 1.

Table 1. Silicon photodiodes used in the measurement. Size and thickness refer to the active volume.

Manufacturer	Type	Size in mm^2	Nominal thickness in μm
Canberra	PIPS	50	300
Canberra	PIPS	50	500
IRD	AXUV	100	27

2.5. Free air ionization chamber PK100

In a strongly simplified model the PK100 free air ionization chamber (FAC) is a parallel plate capacitor filled with ambient air. The beam axis of the measured radiation is in the centre between the electrode plates which have a separation distance of 23.4 cm. One of the plates is subdivided into a large guard that enframes the rectangular collector electrode of length $l = 2.002$ cm in beam direction and a height of 24.0 cm. The guard and collector are separated by a narrow gap of 1 mm and they are kept on ground potential, whereas the opposite electrode is set to a potential of typically $U_c = 6000$ V, so that the ion pairs generated by interactions of photons with air are separated and the current carried by positive ions is recorded by an electrometer.

2.5.1. Free air ionization chamber PK100 as the primary standard in dosimetry. The application of the PK100 in x-ray dosimetry as well as in x-ray radiometry is based on two conditions, namely *secondary electron equilibrium*, i.e. balance of the energy transported by secondary electrons leaving the collection volume and those entering, and complete dissipation of the kinetic energy transferred to secondary electrons in air. These requirements define the upper energy limit up to which the PK100 is a viable primary standard. The lower limit is given by the attenuation of the photon beam between the collector volume and the aperture which defines the reference plane. The PK100 is used as a primary standard in dosimetry in the range of 10 to 100 kV x-ray tube voltages at PTB (Engelke *et al* 1988, Büermann *et al* 2006).

2.5.2. Application of the PK100 in the experiment. In its standard mode of operation the PK100 is used to measure air kerma. In this mode the measuring volume of the chamber is defined by the length of the collector electrode l and the area of the aperture which reduces the photon beam diameter. In the present experiment, however, the diameter of the photon beam is smaller than the aperture and, in addition, is not known precisely enough to define a measuring volume. Consequently the air kerma cannot be obtained, since this needs the energy deposited in air to be divided by the mass. However, for the purpose of this experiment it is sufficient to determine the energy deposited in air across the length l of the collecting electrode. In the following it is described how this quantity can be obtained from the charge measured by the free air chamber. Under conditions of transient secondary electron equilibrium the total charge Q_l collected in the ionization volume of the free air chamber is a measure of the total charge liberated in photon interactions over the length l of the collecting region (Burns and Büermann 2009), and the number of charges per mass can be written as $Q_l/(\rho l)$, where ρ is the density of air. The mean transferred energy R_{en} is obtained by

$$\frac{R_{en}}{\rho l} = \frac{Q_l}{\rho l} \times c(E) \tag{7}$$

Table 2. Values of the correction factors for the humidity k_h, for scattering k_{sc}, and for initial and volume recombination k_{si} and k_{sv} for various photon energies. For k_{sv} at 30 keV the larger value, which is valid for the direct measurements, is given.

k_i	10 keV	30 keV	60 keV
k_h	0.9988(9)	0.9988(9)	0.9988(9)
k_{sc}	0.9877(10)	0.9938(10)	0.9963(10)
k_{si}	1.0006(5)	1.0006(5)	1.0006(5)
k_{sv}	1.0012(1)	1.00063(7)	1.00009(1)

where $c(E)$ is a function which converts the measured charge Q_l into the mean transferred energy R_{en} and E is the energy of the photon. The conversion function can be written as

$$c(E) = \frac{W_{\text{eff}}(E)}{e} \times \prod_i k_i(E) \tag{8}$$

where $W_{\text{eff}}(E)$ is the effective mean energy to produce an ion pair in air (see section 3), e is the elementary charge, and k_i are correction factors to be applied in order to take into account various effects observed for a real free air chamber in contrast to an ideal free air chamber (see section 2.6).

2.6. Correction factors for the free air ionization chamber

The currents measured with an FAC need corrections for several effects. A detailed discussion of the humidity correction k_h, the ion recombination corrections k_{sv} and k_{si}, the correction k_{sc} for additional ionization due to scattered photons, and the correction k_a for attenuation of the photon beam along the collection electrode can be found in the work of Büermann *et al* (2006). Only a short discussion of these effects is included here for this reason and table 2 gives an overview of the values that the correction factors assume at various energies. In contrast to standard measurements using the PK100, the photon beam in use was much smaller than the aperture diameter. Hence, corrections for interactions in the aperture are not needed and the centre of the measuring volume was chosen as the reference point of the FAC. Therefore the classical correction for air attenuation between the reference plane and the centre of the measuring volume is not necessary. The correction of the air attenuation across the length of the collecting electrode discussed by Büermann *et al* (2006) is only needed for photon energies below about 5 keV and was taken to be equal to 1 for the photon energy range used in this work.

The experiment was conducted using atmospheric air with a relative humidity of 70(20)%. whereas the mass energy-absorption coefficient for dry air is the quantity of interest. Therefore a *humidity correction* factor $k_h = 0.9988(9)$ is applied to the ionization current following the recommendation in ICRU (1979).

The *scattering correction* factor k_{sc} takes into account the energy deposited in the measurement volume in reactions of photons that were created by the original beam (e.g., in Compton or elastic scattering) upstream of the interaction region. The scattering correction factor covers a range from 0.9863(10) to 0.9963(10) for photon energies between 8 and 60 keV as was found in Monte Carlo simulations using the EGS code (Kawrakow and Rogers 2000).

The mechanisms of ion recombination in FACs were reviewed by Boag (1987) and are generally divided into two processes: initial recombination and volume recombination, depending on the origin of the ions recombining. *Initial recombination* is not dependent on the intensity of ionizing radiation as it occurs between ions formed from a single ionizing particle. The ion density along one particle's track and the gradient of the electric field perpendicular to the track define the amount of initial recombination. The correction factor k_{si} for initial

recombination of the PK100 was derived to be 1.0006(5) as given in Büermann *et al* (2006) for the electric field applied in the measurements.

Volume (or general) recombination, on the other hand, refers to reactions between positive and negative ions from tracks of different ionizing particles. The probability of this effect increases with the number of particle tracks which is observed as an increase in ionization current. The method of derivation has been described in Büerman *et al* (2006) and yielded $k_{sv} = I_0/I = 1 + \text{const/U}^2 \times \text{I}$ where $\text{const/U}^2 = 4.04 \times 10^7\ \text{A}^{-1}$ and I is the measured ionization current used as a good approximation of the saturation value of ionization current, I_0, in the right-hand expression. The correction for volume recombination does not exceed the value of $k_{sv} = 1.0012(1)$ at 10 keV for the data presented here.

3. Effective mean energy for electron-ion-pair creation in air

When a fast electron is completely stopped in a gaseous medium, ion pairs are created along its path. The mean number of ion pairs N depends on the kinetic energy T of the electron at the beginning and defines the ratio $W = T/N$ (ICRU 2011), the mean energy expended to form an ion pair in gas. For electrons released in interactions with photons of energy E an effective value $W_{\text{eff}}(E)$ can be defined by averaging over the spectral fluence $\text{d}\phi/\text{d}T$ of electrons liberated by photon interactions in air. The effective value is then given by

$$W_{\text{eff}}(E) = \frac{\int_0^{\hat{E}} \left(\frac{\text{d}\phi}{\text{d}T}\right) T \,\text{d}T}{\int_0^{\hat{E}} \left(\frac{\text{d}\phi}{\text{d}T}\right) \frac{T}{W(T)} \,\text{d}T} \tag{9}$$

where $\hat{E}$ is the maximum energy that can be transferred to electrons by photoelectric absorption of photons of energy E. The W value of air increases significantly for electron energies below about 3 keV which results in W_{eff} being photon–energy dependent as well. To determine $W_{\text{eff}}(E)$ we use a parameterization of the W value based on a fit to experimental data from 14.7 to 30.7 eV published by Combecher (1980), from 30 to 601 eV by Waibel and Grosswendt (1978), and from 1.0 to 7.1 keV by Büermann *et al* (2006). The data of Waibel and Grosswendt had to be corrected according to the recommendation of ICRU (1979) because it was not measured for dry air. The asymptotic value for high electron energies was forced to equal $W_{\text{air}}/e = 33.97$ J/C, the value of W_{eff} at high photon energies determined for ^{60}Co radiation (Boutillon and Peroche-Roux 1987). The parameterization yields

$$W(T) = W_{\text{air}} \times (1 - (T/A_1)^{A_2 + T \times A_3})^{-1} \tag{10}$$

with $A_1 = 14.636(29)$ eV, $A_2 = -0.828(4)$, and $A_3 = -3.8(6) \times 10^{-5}\ \text{eV}^{-1}$, which is defined for electron energies $T > A_1$, whereas no ion pairs are formed by electrons with energies below A_1, which closely coincides with the ionization threshold of air molecules.

For photons of less than 100 keV energy transfer to electrons in air occurs either by photoabsorption or by Compton scattering. By incorporating these two effects in a definition similar to the model used by Büermann *et al* (2006) one obtains W_{eff} as the ratio of average energy transferred and average number of ion pairs produced:

$$W_{\text{eff}}(E) = \frac{\sum_{i,J} \left(\frac{c_i \sigma_i}{\sigma}(E)\right) \left[\left(\frac{\sigma_{i,J}^{\text{pe}}}{\sigma_i}(E)\right)\left(T_{i,J}^{\text{pe}} + p_{i,J}^{\text{nr}} T_{i,J}^{\text{nr}}\right) + \omega_{i,J}\left(\frac{\sigma_i^{\text{Ce}}}{\sigma_i}(E)\right)\left(T_{i,J}^{\text{Ce}} + p_{i,J}^{\text{nr}} T_{i,J}^{\text{nr}}\right)\right]}{\sum_{i,J} \left(\frac{c_i \sigma_i}{\sigma}(E)\right) \left[\left(\frac{\sigma_{i,J}^{\text{pe}}}{\sigma_i}(E)\right)\left(\frac{T_{i,J}^{\text{pe}}}{W(T_{i,J}^{\text{pe}})} + p_{i,J}^{\text{nr}} \frac{T_{i,J}^{\text{nr}}}{W(T_{i,J}^{\text{nr}})} + q_{i,J}\right) + \omega_{i,J}\left(\frac{\sigma_i^{\text{Ce}}}{\sigma_i}(E)\right)\left(\frac{T_{i,J}^{\text{Ce}}}{W(T_{i,J}^{\text{Ce}})} + p_{i,J}^{\text{nr}} \frac{T_{i,J}^{\text{nr}}}{W(T_{i,J}^{\text{nr}})} + q_{i,J}\right)\right]} \tag{11}$$

where c_i is the fraction by number of an atomic species (N, O, Ar) in air, and σ and σ_i the total photon cross sections of air and the individual atomic species, respectively. $\sigma_{i,J}^{\text{pe}}$ is the photoabsorption cross section of atom i for shell J, and σ_i^{Ce} the cross section for Compton

Table 3. Constants used in equation (11). All energies are given in keV.

Species	c_i	Shell J	$\omega_{i,J}$	$p^{\mathrm{nr}}_{i,J}$	$E^{\mathrm{B}}_{i,J}$	$T^{\mathrm{nr}}_{i,J}$	$q_{i,J}$
N	0.7848	K	2/7	0.996	0.41	0.37	2
		L	5/7	–	0.02	–	1
O	0.2105	K	1/4	0.994	0.54	0.50	2
		L	3/4	–	0.02	–	1
Ar	0.0047	K	1/9	0.885	3.18	2.70	4.3
		L	4/9	1	0.26	0.23	2.3
		M	4/9	–	0.02	–	1

scattering, which is weighted by $\omega_{i,J}$ for the number of electrons in a particular shell J in an atom of species i based on the assumption of equal cross section for Compton scattering for all electrons of an atom of type i. All cross sections were taken from the EPDL97 database (Cullen *et al* 1997). All properties, e.g. the cross sections and binding energies, were averaged over the respective L or M shells. The values of the constants used in equation (11) are given in table 3. The fraction of non-radiative, e.g. Auger processes in case of lower shell vacancies is given for each atom i and shell J by $p^{\mathrm{nr}}_{i,J}$. The energy of the electron released in the interaction with the primary photon in the case of photoionization and Compton scattering is given by $T^{\mathrm{pe/Ce}}_{i,J} = E_e - E^{\mathrm{B}}_{i,J}$ where $E^{B}_{i,J}$ is the binding energy of the electron in the atom and shell from which it originated and E_e the energy transferred in the photon interaction. For photoionization E_e equals E, while for Compton scattering E_e is dependent on the deflection angle of the scattered photon. Therefore, the expression $\frac{T^{Ce}_{i,J}}{W(T^{Ce}_{i,J})}$ is averaged over the deflection angles by numerical integration of the Klein–Nishina differential cross section for Compton scattering. Values of $E^{\mathrm{B}}_{i,J}$, $p^{\mathrm{nr}}_{i,J}$, and $T^{\mathrm{nr}}_{i,J}$ were calculated from the EADL database (Perkins *et al* 1991).

As discussed in section 2.5.2 in this measurement the mean transferred energy is derived from the number of detected positive charges by multiplication with $W_{\mathrm{eff}}(E)$. However, in addition to the ion pairs created by the electrons set in motion by the primary photon interaction, further charge carriers are released as a result of the primary photon interaction itself. These are the secondary electrons released through the photoabsorption or Compton process (Büermann *et al* 2006), electrons of the same atom or molecule that are released in the subsequent deexcitation by non-radiative (e.g. Auger) decay cascades (Takata and Begum 2008), and the residual ion, which is multiply charged if non-radiative processes occur. While the ion pairs produced by the Auger electrons also contribute to the mean transferred energy, the charge of the residual ions must not be counted for this purpose. The average number of electrons $q_{i,J}$ released from the atom in the primary photon interaction (and thus the surplus charges detected) was taken from the study of Takata and Begun (2008) and included in table 3. This excess charge is taken into account by $q_{i,J}$ in equation (11).

Therefore, W_{eff} as given by equation (11) is the appropriate factor to be used in equation (8). The ratio of W_{eff} and W_{air}, as a constant approximation for W_{eff}, is shown in figure 1 for the range of 3 to 100 keV. The difference between the two is smaller than 1% for photon energies above 5 keV.

4. Measurements

4.1. Measurement equation

Replacing the energies R and R_{en} by their derivatives with respect to time, one can rewrite equation (4) in terms of the radiant power $P = \dot{R}$ and the mean transferred power

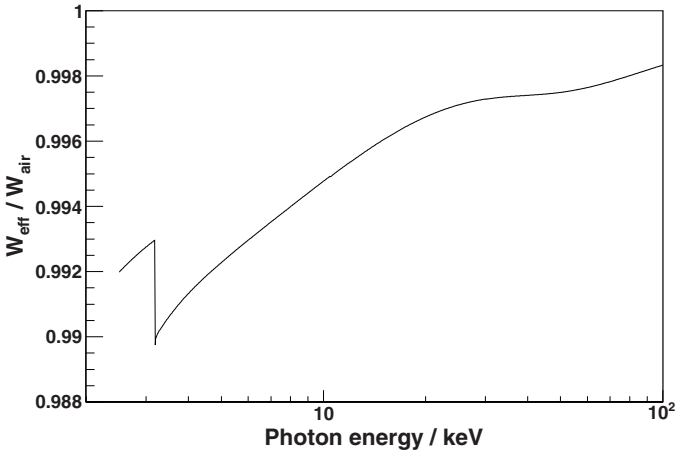

Figure 1. The total correction implied by the energy dependent value of W_{eff} (equation (11)).

$P_{\mathrm{en}} = \dot{R}_{\mathrm{en}}$ as

$$\frac{\mu_{en}}{\rho} = \frac{1}{\rho\,\mathrm{d}l}\frac{\mathrm{d}P_{\mathrm{en}}}{P} \tag{12}$$

as a representation of the mass energy-absorption coefficient, which describes more accurately the experimental conditions.

When the radiant power or energy flux P is measured using the cryogenic radiometer directly, P can be expressed by equation (6). In the case of indirect measurements with a calibrated photodiode as a transfer standard the expression changes to

$$P = I_D/s \tag{13}$$

where I_D is the current of the photodiode when exposed to the photon beam corrected for the dark current and s is its responsivity which is determined by calibration as described in section 4.3.1.

The free air ionization chamber measures a current $I_l = \dot{Q}_l$, which yields

$$\frac{\mathrm{d}P_{\mathrm{en}}}{\rho\,\mathrm{d}l} = \frac{I_l}{\rho\,\mathrm{d}l}\frac{W_{\mathrm{eff}}}{W_{\mathrm{air}}}\frac{W_{\mathrm{air}}}{e} \times k_{\mathrm{h}} \times k_\rho \times k_{\mathrm{sc}} \times k_{\mathrm{si}} \times k_{\mathrm{sv}} \times k_{\mathrm{other}} \tag{14}$$

based on equation (7), where k_{other} contains several factors, among which electric field distortions resulting in an uncertainty of the interaction length and the effect of the polarity of the bias voltage are the dominant ones. This factor also includes the uncertainty of the photon energy. Together with equation (6), the measurement equation for the direct comparison between FAC and SYRES I can be expressed as

$$\frac{\mu_{en}}{\rho} = \frac{\alpha_{Cav}}{P_{\mathrm{el}}}\frac{I_l}{\rho\,\mathrm{d}l}\frac{W_{\mathrm{eff}}}{W_{\mathrm{air}}}\frac{W_{\mathrm{air}}}{e} \times k_{\mathrm{h}} \times k_\rho \times k_{\mathrm{sc}} \times k_{\mathrm{si}} \times k_{\mathrm{sv}} \times k_{\mathrm{Be}} \times k_{\mathrm{pos}} \times k_{\mathrm{other}} \tag{15}$$

where k_{Be} and k_{pos} are correction factors for the transmittance of a beryllium window and the different positions of the free air chamber and the radiometer, respectively, which are discussed together with the specific setup (section 4.2). In measurements using the calibrated photodiodes, this is replaced by

$$\frac{\mu_{\mathrm{en}}}{\rho} = \frac{s_D}{I_D}\frac{I_l}{\rho\,\mathrm{d}l}\frac{I_M^D}{I_M^{PK}}\frac{W_{\mathrm{eff}}}{W_{\mathrm{air}}}\frac{W_{\mathrm{air}}}{e} \times k_{\mathrm{h}} \times k_\rho \times k_{\mathrm{sc}} \times k_{\mathrm{si}} \times k_{\mathrm{sv}} \times k_{\mathrm{other}} \tag{16}$$

which is discussed in detail in section 4.3.

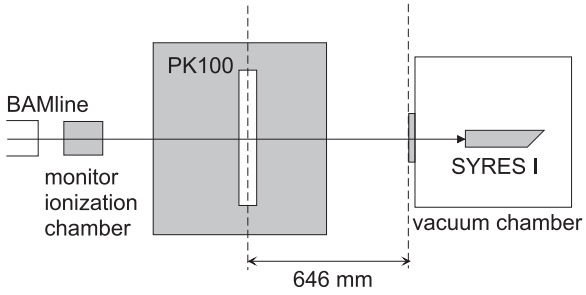

Figure 2. Setup for measurements directly comparing mean transferred power and radiant power as used in the range of 30 to 60 keV photon energy.

4.2. Setup for direct comparison of SYRES I and PK100 (30 –60 keV)

Since the measurement with the PK100 is in a sense non-destructive it is possible to perform simultaneous measurements of the photon beam with the FAC and the cryogenic radiometer. In measurements for photon energies in the range of 30 to 60 keV the mean transferred power and the radiant power were compared directly using a setup as shown in figure 2 with a beryllium entrance window to the vacuum vessel containing SYRES I 646(3) mm downstream of the centre of the PK100 measurement volume.

The main advantage of this method is evident as it allows a reference of the results obtained with the most precise devices to each other without any uncertainty originating from the photodiodes as transfer standards. However, the radiant power at the two devices is different, as the two measurements here are not performed at the same spot, but with a considerable distance for the photons to travel in air and the thin entrance window into the vacuum vessel separating the two detectors. For monoenergetic photon beams the dominant effect of this is an attenuation that needs to be measured, modelled, or calculated, which can be done with sufficiently low uncertainty for high energy photons. By calculation, the beryllium window of a thickness of 0.400(25) mm was found to incur a correction of $k_{\mathrm{Be}} = 1.0144(9)$ at 30 keV photon energy, while yielding smaller values at higher energies.

For low-energy photons the attenuation in air leads to correction factor deviating significantly from unity and introducing an enhanced uncertainty which discouraged measurements using this setup at energies lower than 30 keV. Above 60 keV the absorption coefficient of the cryogenic radiometer drops below 0.995 owing to transmission of photons through the base plate at the rear end of the absorber cavity. Furthermore, due to variations of its thickness, the absorption coefficient becomes position dependent across the base plate. This introduces an uncertainty to the measurement which is too large to achieve the desired low-uncertainty data (Gerlach *et al* 2008).

4.3. Setup for indirect comparison of the mean transferred power and the radiant power (8 –30 keV)

Indirect comparisons of the mean transferred power and the radiant power for energies up to 30 keV were undertaken in two steps using several semiconductor photodiodes. In the first step these were calibrated against the cryogenic radiometer SYRES I. In the second step they were used to determine the radiant power while intermittently the mean transferred power was measured in the PK100. This intermediate step is necessary, because at the relatively low

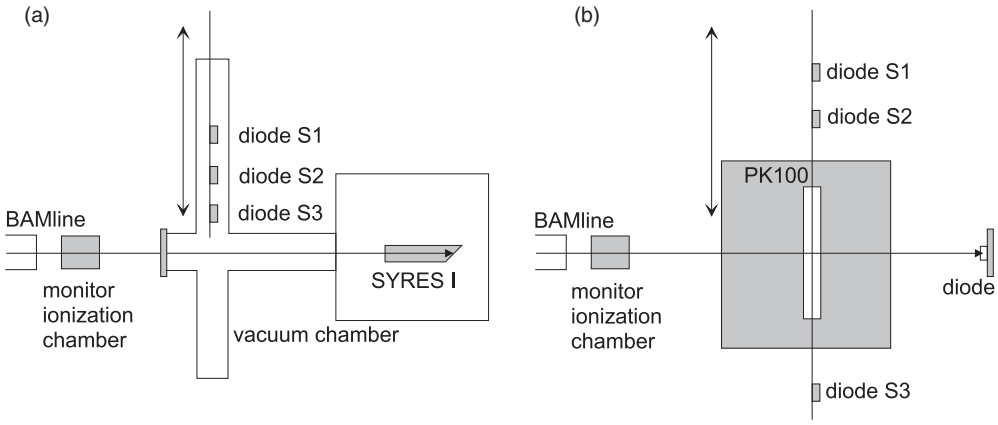

Figure 3. Setup for measurements indirectly comparing mean transferred power and radiant power as used in the range of 8 to 30 keV photon energy: (a) for the calibration of the photodiodes (b) for the measurement.

photon energies attenuation in air over a distance of 646 mm becomes very large. Because the SYRES I setup is not meant to be easily moveable and it needs to be operated under vacuum while the PK100 needs to be operated at ambient pressure, it was not feasible to operate them under conditions where the x-ray photons need to travel a smaller (or even zero) distance in air between the measurement positions of the two devices. The photodiodes, however, can be operated in air and in vacuum and therefore help to overcome the problem of attenuation by using a setup as discussed in the following.

4.3.1. Calibration of the semiconductor photodiodes. The calibration was done using a setup as shown in figure 3(a). All devices were kept in a common vacuum vessel so that attenuation could be neglected. The photon flux was recorded using the monitor chamber. Normalization to this relative measurement compensates the change of photon flux between sequential measurements with different diodes. The specific semiconductor photodiode responsitivities s_D were obtained as

$$s_D = \frac{I_D/I_M^{(D)}}{P_{el}/I_M^{(C)}} \times \alpha_{Cav} \tag{17}$$

where $I_D/I_M^{(D)}$ is the ratio of radiation induced diode current to current in the monitor chamber during the measurement with a diode, $P_{el}/I_M^{(C)}$ the ratio of electrical substitution power at the cryogenic radiometer to monitor current while measuring at SYRES I, and α_{Cav} is the absorption coefficient of the cavity.

4.3.2. Measurement of the mean transferred power versus photodiode current. In another set of measurements alternately the mean transferred power was measured using the PK100 FAC or the radiant power was measured using the three calibrated semiconductor photodiodes one after the other. The four devices were mounted next to each other on a translation stage to be able to position the centres of their respective measurement volumes at the same measurement point in order to avoid differences in air attenuation (figure 3(b)).

Table 4. The uncertainty budget of the measurement of μ_{en}/ρ at photon energies of 30 keV (direct) according to GUM (ISO 2008), using uniform or normal probability distributions as appropriate. X_i is ith quantity, x_i its value, $u(x_i)$ the corresponding relative standard uncertainty, c_i the related sensitivity coefficient and u_c the total relative uncertainty of μ_{en}/ρ.

X_i	x_i	$u(x_i)$/%	$c_i u(x_i)/(\mathrm{cm}^2\ \mathrm{g}^{-1})$	$((c_i u(x_i))^2/u_c^2)^{1/2}$/%
P	5.738×10^{-6} W	0.12	-1.7×10^{-4}	5.1
I_l	1.455×10^{-10} A	0.26	3.8×10^{-4}	24.1
ρ_0	1.2046×10^{-3} g cm^{-3}	0.01	-1.5×10^{-5}	0.0
l	4.997 cm	0.02	-3.0×10^{-5}	0.1
W_{air}	33.97 eV	0.32	4.8×10^{-4}	38.9
$W_{\mathrm{eff}}/W_{\mathrm{air}}$	0.9973	0.1	1.5×10^{-4}	3.7
k_ρ	1.0103	0.05	7.4×10^{-5}	0.9
k_{sc}	0.9938	0.1	1.5×10^{-4}	3.8
k_{Be}	1.0144	0.09	1.3×10^{-4}	2.9
k_{h}	0.9988	0.09	1.3×10^{-4}	3.0
k_{pos}	1.0276	0.02	2.9×10^{-5}	0.1
k_{sv}	1.00063	0.007	1.0×10^{-5}	0.0
k_{si}	1.0006	0.05	7.5×10^{-5}	0.9
k_{other}	0.9990	0.21	3.1×10^{-4}	16.4
Result	value	u_c/%		
μ_{en}/ρ	0.1492 cm^2 g^{-1}	0.52		

The normalization of the mean transferred power to radiant power was done by averaging over all three diode measurements (see also equation (16))

$$\frac{\mu_{\mathrm{en}}}{\rho} = \sum_D \left(w_D \times \frac{I_l/I_M^{PK}}{I_D/I_M^D} \times \frac{W_{\mathrm{eff}}/e}{\rho_{\mathrm{air}}(p,T)} \times \frac{s_D}{l} \times \prod_j k_j \right) \tag{18}$$

where D is the label for the respective semiconductor photodiode, w_D the corresponding statistical weight of the measurement with $\sum_D w_D = 1$, I_l and I_D the radiation induced electric currents measured at the FAC and the diode labelled D, respectively. l denotes the length of interaction region in the FAC. The monitor currents I_M^{PK} and I_M^D were used to relate the measurements of the mean transferred power and the radiant power which did not happen simultaneously but rather sequentially. $\prod_j k_j$ is the product of the various correction factors listed in equation (16).

4.4. Uncertainties

The uncertainties were estimated according to the 'Guide to the expression of uncertainty in measurement' (GUM, ISO 2008) and are given in table 4 for the direct measurement at 30 keV as an example.

The beryllium window correction is based on calculations. Its thickness was experimentally determined by earlier measurements. The uncertainty of the correction $k_{\mathrm{Be}} = 1.0144(9)$ is dominated by the uncertainty of the thickness of the window of 0.400(25) mm. The correction for the air attenuation induced by the different positions of the measurement of the mean transferred power and the radiant power, k_{pos}, was calculated from the distance between the measurement points, or more specifically, from the centre of the measurement electrode in the free air chamber to the beryllium window, the density of the air as derived from the measured pressure and air temperature and the tabulated values of the mass attenuation coefficient of air of the XCOM database (Berger *et al* 2010). The uncertainty of the mass attenuation coefficient of 1% is the dominant contribution to the uncertainty of k_{pos}.

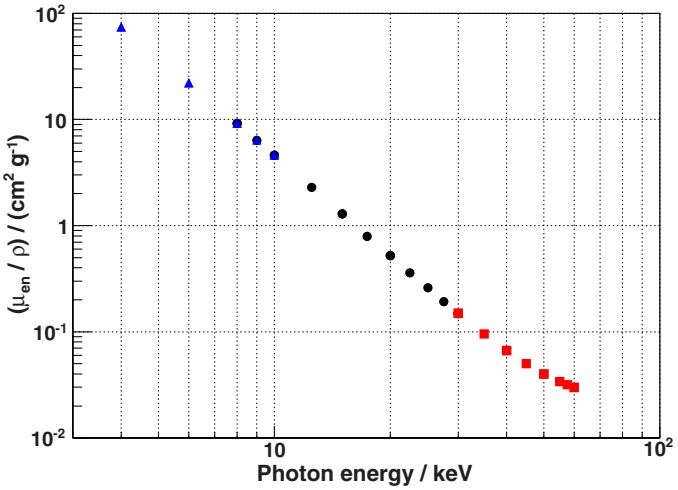

Figure 4. The mass energy-absorption coefficient μ_{en}/ρ as a function of the photon energy E as obtained in indirect measurements using various photodiodes (black circles) and direct measurement (red squares). Results from a previous measurement (Büermann *et al* 2006) with the new and revised correction factors applied are shown as blue triangles. The uncertainties are smaller than the markers.

4.4.1. Uncertainties in the measurement using the free air chamber. The dominant uncertainty in the measurement of mean transferred power to air in the free air chamber PK100 is the W value of air which is given as $W_{\text{air}} = 33.97$ eV with a relative uncertainty of 0.32% (Burns 2012). The effective W value W_{eff} is influenced by the choice of the parameterization of the W-value for electrons and the constants given in table 3. The uncertainty of the parameter values of W_{eff} (equation (10)) contributes very little to the uncertainty of the correction: the maximum contribution for photon energies above 10 keV is about 0.02% to the ratio $W_{\text{eff}}/W_{\text{air}}$. The value of this ratio agrees very well–better than 0.001 for photon energies above 10 keV–with the correction factor suggested by Takata and Begum (2008) based on a different parameterization. This 0.1% is the uncertainty that we attribute to this correction.

In k_{other} several factors and their uncertainties are grouped together, mainly electric field distortions resulting in an additional uncertainty of the interaction length and the effect of the polarity of the bias voltage. In addition, the uncertainty of the photon energy calibration of 15 eV is included here.

For the ionization current measurement the statistical uncertainty is 0.05% while the calibration of the amperemeter gives rise to another contribution of 0.25% where the dominant source is the non-linearity.

4.4.2. Uncertainties in the measurement of the radiant power. The uncertainty of the measurement of the radiant power is discussed in detail by Gerlach *et al* (2008). The value given there and cited here includes the uncertainty of the absorptance.

5. Results and discussion

The mass energy-absorption coefficients as obtained in indirect and direct measurements are shown in figure 4 in double logarithmic scale. A smooth decrease following roughly a $1/E^2$

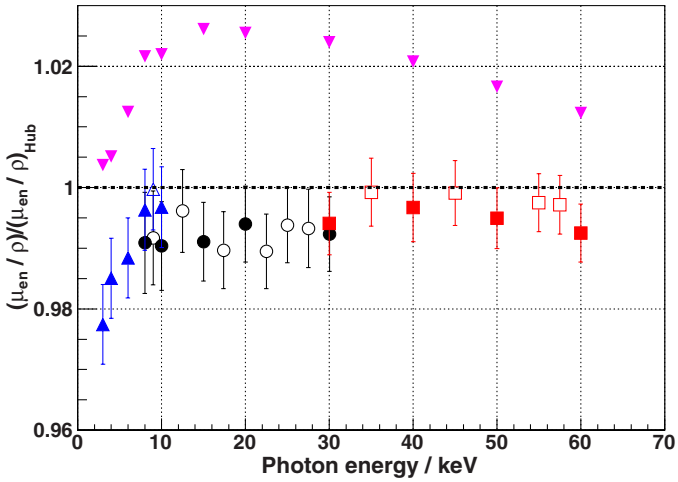

Figure 5. The mass energy-absorption coefficient μ_{en}/ρ as obtained in direct measurements (red squares) and in indirect measurements with calibrated photodiodes (black circles). The average value for all photodiodes at the same energy is shown with the standard deviation of the single measurement values as uncertainty, unless this is smaller than the smallest uncertainty of an individual measurement. The blue upward triangles indicate selected results published in Büermann *et al* (2006) with revised corrections (appendix). The magenta downward triangles are values calculated by Seltzer (1993). All data are normalized to the calculated values of Hubbell (1982). Open symbols indicate that for the corresponding data point normalization had to be done to an interpolation of published data.

dependence between 4 and 40 keV is found as expected from the underlying cross sections. For a more detailed discussion and the comparison to calculations based on theoretical data (Hubbell 1982, Seltzer 1993), figure 5 presents the data normalized to the mass energy-absorption coefficient μ_{en}/ρ provided by Hubbell (1982). For photon energies for which no value of μ_{en}/ρ is provided in that work, an interpolation between given values is used which might introduce an uncertainty that appears to be below 0.5% even for energies above 40 keV, but that was not accounted for in the depicted experimental uncertainties in figure 5.

The data from direct and indirect measurements depict a smooth curve for the whole range of 8 to 60 keV. At 30 keV, where the energy ranges overlap, the agreement is very good, proving that the experimental methods yield consistent results. For 8 to 10 keV experimental data from the earlier measurement is available for comparison (Büermann *et al* (2006)). Within the uncertainty, this data also agrees well with the indirect measurements of this work. Thus, consistent experimental data is now available from 3 to 60 keV.

For photon energies between 8 and 60 keV there is a difference of 1.5%-3.5% between the experimental results and the calculations of Seltzer (1993), which correspond to the widely accepted XCOM data (Berger *et al* 2010), whereas the experimental data agree within 1% with the Hubbell calculations, both for direct and indirect measurements. The measured values of μ_{en}/ρ are tabulated in table 5 together with the corresponding values given by Hubbell (1982) and Seltzer (1993), if they exist, and their relative deviations from the experimental values.

According to Seltzer (1993), the main differences between his calculations and those of Hubbell (1982) are found in the photoelectric absorption cross sections applied. In both cases, the photoabsorption cross sections are based on theoretical cross section data provided by Scofield (1973) in the energy range above 1 keV. The Seltzer data use the original theoretical cross sections provided by Scofield (1973) while ignoring the re-normalization

Table 5. The measured values of μ_{en}/ρ in comparison to calculations of Hubbell (1982) and Seltzer (1993). Δ is the relative deviation of the calculation from the experimental value, normalized to the latter.

Energy (keV)	(μ_{en}/ρ)/(cm^2 g^{-1}) This work	(μ_{en}/ρ)/(cm^2 g^{-1}) Hubbell (1982)	(μ_{en}/ρ)/(cm^2 g^{-1}) Seltzer (1993)	Δ/% to Hubbell (1982)	Δ/% to Seltzer (1993)
8.000	$9.162(77) \times 10^{0}$	9.246×10^{0}	9.446×10^{0}	0.9	3.1
9.000	$6.375(50) \times 10^{0}$	–	–	–	–
10.00	$4.595(34) \times 10^{0}$	4.640×10^{0}	4.742×10^{0}	1.0	3.2
12.50	$2.296(16) \times 10^{0}$	–	–	–	–
15.00	$1.288(8) \times 10^{0}$	1.300×10^{0}	1.334×10^{0}	0.9	3.6
17.47	$7.959(73) \times 10^{-1}$	–	–	–	–
20.00	$5.223(33) \times 10^{-1}$	5.255×10^{-1}	5.389×10^{-1}	0.6	3.2
22.50	$3.598(22) \times 10^{-1}$	–	–	–	–
25.01	$2.592(16) \times 10^{-1}$	–	–	–	–
27.51	$1.933(13) \times 10^{-1}$	–	–	–	–
30.00	$1.492(8) \times 10^{-1}$	1.501×10^{-1}	1.537×10^{-1}	0.6	3.0
35.00	$9.566(54) \times 10^{-2}$	–	–	–	–
40.00	$6.672(38) \times 10^{-2}$	6.694×10^{-2}	6.833×10^{-2}	0.3	2.4
45.00	$5.019(27) \times 10^{-2}$	–	–	–	–
50.00	$4.011(20) \times 10^{-2}$	4.031×10^{-2}	4.098×10^{-2}	0.5	2.2
55.00	$3.387(16) \times 10^{-2}$	–	–	–	–
57.50	$3.168(15) \times 10^{-2}$	–	–	–	–
60.00	$2.981(14) \times 10^{-2}$	3.004×10^{-2}	3.041×10^{-2}	0.8	2.0

factors suggested in that work. The older data by Hubbell (1982) has the re-normalization applied, but it cannot be excluded that adjustments were made to fit experimental results in the low-energy region (Hubbell 1977). In a later work, Hubbell (1999) recommends using the mass energy-absorption coefficients by Seltzer (1993), because these are supposed to describe low-energy (below 100 keV) experimental cross section data better.

6. Summary

The mass energy-absorption coefficient μ_{en}/ρ of air for photon energies between 10 and 60 keV has been measured for the first time with an uncertainty below 1%. The experiments were performed by PTB at a wavelength-shifter beamline at the electron storage ring BESSY II using monochromatized synchrotron radiation, and the high accuracy primary standards for radiant power (the cryogenic radiometer SYRES I) and air kerma (the free air ionization chamber PK100). The resulting relative standard uncertainties are in the range of 0.5% to 0.8%, considerably better than what is assumed for calculated data. The results do not agree well with the widely accepted XCOM calculation (Seltzer 1993), but show reasonably good agreement with calculations published earlier by Hubbell (1982).

Acknowledgment

The experimental assistance of Reinulf Böttcher, Levent Cibik, Ulf Knoll and Peter Müller is gratefully acknowledged.

Appendix. Improved values of μ_{en}/ρ for 3 to 10 keV photons

In the context of this work (section 3) we re-evaluated the correction for electrons being released in the primary interactions that was published in Büermann *et al* (2006) on the basis

Table A1. Improved values (with respect to Büermann *et al* (2006)) of the measured values of μ_{en}/ρ.

E (eV)	μ_{en}/ρ (cm^2 g^{-1})	E (eV)	μ_{en}/ρ (cm^2 g^{-1})	E (eV)	μ_{en}/ρ (cm^2 g^{-1})	E (eV)	μ_{en}/ρ (cm^2 g^{-1})
3000.0	157.17	3205.8	145.95	5000.0	38.42	7800.0	9.93
3100.0	142.63	3206.0	145.97	5100.0	36.22	7900.0	9.565
3195.0	130.22	3207.0	145.46	5200.0	34.16	8000.0	9.212
3196.0	130.40	3208.0	145.23	5300.0	32.25	8100.0	8.868
3197.0	130.25	3209.0	145.11	5400.0	30.50	8200.0	8.543
3198.0	130.22	3210.0	144.73	5500.0	28.85	8300.0	8.226
3199.0	130.35	3211.0	144.63	5600.0	27.30	8400.0	7.934
3200.0	130.27	3212.0	144.39	5700.0	25.88	8500.0	7.648
3201.0	130.54	3213.0	144.09	5800.0	24.56	8600.0	7.373
3202.0	131.44	3214.0	143.79	5900.0	23.31	8700.0	7.119
3202.2	132.13	3215.0	143.67	6000.0	22.16	8800.0	6.871
3202.4	132.87	3300.0	132.43	6100.0	21.11	8900.0	6.636
3202.6	133.86	3400.0	120.84	6200.0	20.07	9000.0	6.427
3202.8	135.42	3500.0	110.97	6300.0	19.10	9100.0	6.196
3203.0	138.27	3600.0	102.39	6400.0	18.22	9200.0	6.010
3203.2	143.45	3700.0	94.30	6500.0	17.36	9300.0	5.798
3203.4	153.39	3800.0	87.12	6600.0	16.59	9400.0	5.614
3203.6	167.88	3900.0	80.68	6700.0	15.84	9500.0	5.430
3203.8	169.44	4000.0	74.83	6800.0	15.15	9600.0	5.254
3204.0	155.81	4100.0	69.24	6900.0	14.46	9700.0	5.089
3204.2	145.78	4200.0	64.59	7000.0	13.84	9800.0	4.926
3204.4	141.15	4300.0	60.24	7100.0	13.27	9900.0	4.766
3204.6	140.21	4400.0	56.35	7200.0	12.70	10000.0	4.625
3204.8	141.84	4500.0	52.66	7300.0	12.18	10100.0	4.480
3205.0	145.88	4600.0	49.30	7400.0	11.69	10200.0	4.345
3205.2	148.20	4700.0	46.23	7500.0	11.21		
3205.4	146.42	4800.0	43.41	7600.0	10.78		
3205.6	145.71	4900.0	40.85	7700.0	10.36		

of the discussion of Takata and Begum (2008). In the latter work it was pointed out that also the charges of Auger electrons being released from the target atom of the primary interaction need to be corrected for, since the charges are measured in an FAC, but are not covered by the definition of air kerma.

In Büermann *et al* (2006) measured values of the mass energy-absorption coefficient in the range of 3 to 10 keV were presented which have now been re-evaluated in light of the improved correction factors (section 3). The revised values are presented in table A1. The ratio of the revised value to the old value ranges between 0.991 at 3.3 keV and 0.996 at 10 keV.

References

Andreo P, Burns D T and Salvat F 2012 On the uncertainties of photon mass energy-absorption coefficients and their ratios for radiation dosimetry *Phys. Med. Biol.* **57** 2117–36

Agostinelli S *et al* 2003 GEANT4–a simulation toolkit *Nucl. Instrum. Methods* A **506** 250–303

Attix F 1979 The partition of kerma to account for bremsstrahlung *Health Phys.* **36** 347–54

Beckhoff B, Gottwald A, Klein R, Krumrey M, Müller R, Richter M, Scholze F, Thornagel R and Ulm G 2009 A quarter-century of metrology using synchrotron radiation by PTB in Berlin *Phys. Status Solidi* b **246** 1415–34

Berger M J, Hubbell J H, Seltzer S M, Chang J, Coursey J S, Sukumar R, Zucker D S and Olsen K 2010 XCOM: Photon Cross Section Database (version 1.5) Available at: http://physics.nist.gov/xcom (Friday 4 May 2012 05:53:30 EDT) (Gaithersburg, MD: National Institute of Standards and Technology)

Boag J W 1987 *The Dosimetry of Ionizing Radiation* vol 2 ed K R Kase, B E Bjarngard and F H Attix (New York: Academic) pp 169–243

Bradley D A, Chang C S, Shukri A, Tajuddin A A and Ghose A M 1989 A new method for the direct measurement of the energy absorption coefficient of gamma rays *Nucl. Instrum. Methods* A **280** 392–4

Büermann L, Grosswendt B, Kramer H-M, Selbach H-J, Gerlach M, Hoffmann M and Krumrey M 2006 Measurement of the x-ray mass energy-absorption coefficient of air using 3 keV to 10 keV synchrotron radiation *Phys. Med. Biol.* **51** 5125–50

Burns D T and Büermann L 2009 Free air ionisation chambers *Metrologia* **46** S9–S23

Burns D T 2012 An analysis of existing data for W_a, the I-value for graphite and the product $W_a s_{c,air}$ *Metrologia* **49** 507–12

Combecher D 1980 Measurement of W values of low-energy electrons in several gases *Rad. Res.* **84** 189–218

Cullen D E, Hubbell J H and Kissel L 1997 EPDL97: the evaluated photon data library *Lawrence Livermore National Laboratory Report UCRL-50400* vol 6 rev 5

Engelke B A, Oetzmann W and Struppek G 1988 Die Meßeinrichtungen der Physikalisch-Technischen Bundesanstalt zur Darstellung der Einheiten der Standard-Ionendosis, Photonen-Äquivalentdosis und Luftkerma *PTB Report PTB-Dos-16* (Braunschweig, PTB)

Gerlach M, Krumrey M, Cibik L, Müller P, Rabus H and Ulm G 2008 Cryogenic radiometry in the hard x-ray range *Metrologia* **45** 577–85

Gerlach M, Krumrey M, Cibik L, Müller P and Ulm G 2009 Comparison of scattering experiments using synchrotron radiation with Monte Carlo simulations using Geant4 *Nucl. Instrum. Methods* A **608** 339–43

Görner W, Hentschel M P, Müller B R, Riesemeier H, Krumrey M, Ulm G, Diete W, Klein U and Frahm R 2001 BAMline: The first hard x-ray beamline at BESSY II *Nucl. Instrum. Methods* A **467-468** 703–6

Hubbell J H 1977 Photon mass attenuation and energy-absorption coefficients for H, C, N, O, Ar and seven mixtures from 0.1 keV to 20 MeV *Radiat. Res.* **70** 58–81

Hubbell J H 1982 Photon mass attenuation and energy-absorption coefficients from 1 keV to 20 MeV *Int. J. Appl. Radiat. Isot.* **33** 1269–90

Hubbell J H 1999 Compilation of photon cross-sections: some historical remarks and current status *X-Ray Spectrom.* **28** 215–23

ICRU 1979 Average energy required to produce an ion pair *ICRU Report 31* (Washington DC: ICRU)

ICRU 2011 Fundamental quantities and units for ionizing radiation *ICRU Report 85* (Washington DC: ICRU)

ISO 2008 Guide to the expression of uncertainty in measurement *(Geneva: International Organization for Standardization)*

Kawrakow I and Rogers D W O 2000 The EGSnrc code system: Monte Carlo simulation of electron and photon transport *NRCC Report* PIRS-701 (Ottawa: National Research Council of Canada)

Krumrey M, Gerlach M, Scholze F and Ulm G 2006 Calibration and characterization of semiconductor x-ray detectors with synchrotron radiation *Nucl. Instrum. Methods* A **568** 364–8

Perkins S T, Cullen D E, Chen M H, Hubbell J H, Rathkopf J A and Scofield J H 1991 Tables and graphs of atomic subshell and relaxation data derived from the LLNL Evaluated Atomic Data Library (EADL), $Z = 1$–100 *Lawrence Livermore National Laboratory Report UCRL-504000* vol 30

Scofield J H 1973 Theoretical photoionization cross sections from 1 to 1500 keV *Lawrence Livermore National Laboratory Report UCRL-51326*

Seltzer S M 1993 Calculation of photon mass energy-transfer and mass energy-absorption coefficients *Radiat. Res.* **136** 147–70

Singh K, Bal H K, Sohal I K and Sud S P 1991 Measurement of energy absorption coefficients at 662 keV in soil samples *Appl. Radiat. Isot.* **42** 1239–40

Takata N and Begum A 2008 Corrections to air kerma and exposure measured with free air ionisation chambers for charge of photoelectrons, Compton electrons and Auger electrons *Rad. Prot. Dos.* **130** 410–8

Waibel E and Grosswendt B 1978 Determination of W values and Backscatter coefficients for slow electrons in air *Radiat. Res.* **76** 241–9